Draft version February 2, 2008
Preprint typeset using LaTeX style emulateapj v. 10/09/06

arXiv:0710.1011v1 [astro-ph] 4 Oct 2007

MEASUREMENTS OF PLASMA MOTIONS IN DYNAMIC FIBRILS

Øystein Langangen, Luc Rouppe van der Voort[1], and Yong Lin
Institute of Theoretical Astrophysics, University of Oslo, P.O. Box 1029 Blindern, N-0315 Oslo, Norway
Draft version February 2, 2008

ABSTRACT

We present a 40 minute time series of filtergrams from the red and the blue wing of the Hα line in an active region near the solar disk center. From these filtergrams we construct both Dopplergrams and summed "line center" images. Several dynamic fibrils (DFs) are identified in the summed images. The data is used to simultaneously measure the proper motion and the Doppler signals in DFs. For calibration of the Doppler signals we use spatially resolved spectrograms of a similar active region. Significant variations in the calibration constant for different solar features are observed, and only regions containing DFs have been used in order to reduce calibration errors. We find a coherent behavior of the Doppler velocity and the proper motion which clearly demonstrates that the evolution of DFs involve plasma motion. The Doppler velocities are found to be a factor 2–3 smaller than velocities derived form proper motions in the image plane. The difference can be explained by the radiative processes involved, the Doppler velocity is a result of the local atmospheric velocity weighted with the response function. As a result the Doppler velocity originates from a wide range in heights in the atmosphere. This is contrasted by the proper motion velocity which is measured from the sharply defined bright tops of the DFs and is therefore a very local velocity measure. The Doppler signal originates from well below the top of the DF. Finally we discuss how this difference together with the lacking spatial resolution of older observations have contributed to some of the confusion about the identity of DFs, spicules and mottles.

Subject headings: Sun: chromosphere — Sun: atmospheric motions

1. INTRODUCTION

The solar chromosphere owes its name to the reddish rim that appears above the lunar limb during solar eclipses. This reddish color mostly stems from the Balmer Hα spectral line which makes this line one of the most important chromospheric diagnostics. Due to the highly dynamic state of the chromosphere and strong NLTE effects, the line formation processes are still not yet fully understood (e.g. Carlsson & Stein 2002; Leenaarts & Wedemeyer-Böhm 2006). This is an important shortcoming in our interpretation tools which makes Hα observations traditionally difficult to interpret.

Due to the highly fibrilar structure of the chromosphere (Hale 1908), a strong influence from magnetic fields on the chromosphere has been suspected for about a century.

The most common of these fibrilar magnetic fine structures are the jet-like structures known as spicules, mottles, and dynamic fibrils (DFs). In short, spicules are traditionally observed at the limb, mottles on disk in the quiet Sun, and DFs in active regions.

Whether or not these structures are manifestations of the same phenomenon viewed at different angles have been the subject of a long standing discussion (e.g. Beckers 1968; Grossmann-Doerth & Schmidt 1992; Tsiropoula et al. 1994; Suematsu et al. 1995; Christopoulou et al. 2001; Rouppe van der Voort et al. 2007). One important argument against these structures being caused by the same mechanism has been the difference in the measured absolute velocities (Grossmann-Doerth & Schmidt 1992). Other authors have done direct measurements of mottles crossing the limb (Christopoulou et al. 2001). They also state that since both proper motions and Doppler motions are used in the comparisons, systematic errors are probably introduced. Such errors might also be amplified by the rather limited spatial resolution of some of the data sets used.

The detailed analysis of DFs has accelerated in recent years (e.g. De Pontieu et al. 2004; de Wijn & de Pontieu 2006; Hansteen et al. 2006; De Pontieu et al. 2007; Heggland et al. 2007) due to major advances in both observational techniques and simulation efforts.

One of the main conclusions from these studies is that DFs are driven by magneto-acoustic shocks caused by p-mode oscillations and convective flows leaking into the chromosphere.

In a recent study, Langangen et al. (2007, from now on paper 1) presented spectroscopic analysis of DFs as seen in one of the Ca II IR lines. Numerical analysis of the line formation process showed a much lower DF velocity derived from Doppler measurements as compared to the proper motion velocity. This was found to be due to both the low formation height and the extensive width of the contribution function of the Ca II IR line. Furthermore, the DFs analyzed in paper 1 showed mass motion, thus ruling out any ionization/temperature wave as explanation model for DFs (e.g. Sterling 2000, and references therein).

With the advantage of well sampled spectral line profiles, the number of analysed DFs in paper 1 was rather modest due to the limited spatial coverage of the spectrograph slit. With the current data we exploit the wide spatial coverage of a tunable filter instrument, at the expense of limited spectral resolution.

Electronic address: oysteol@astro.uio.no
[1] also at Center of Mathematics for Applications, University of Oslo, P.O. Box 1053 Blindern, N-0316 Oslo, Norway

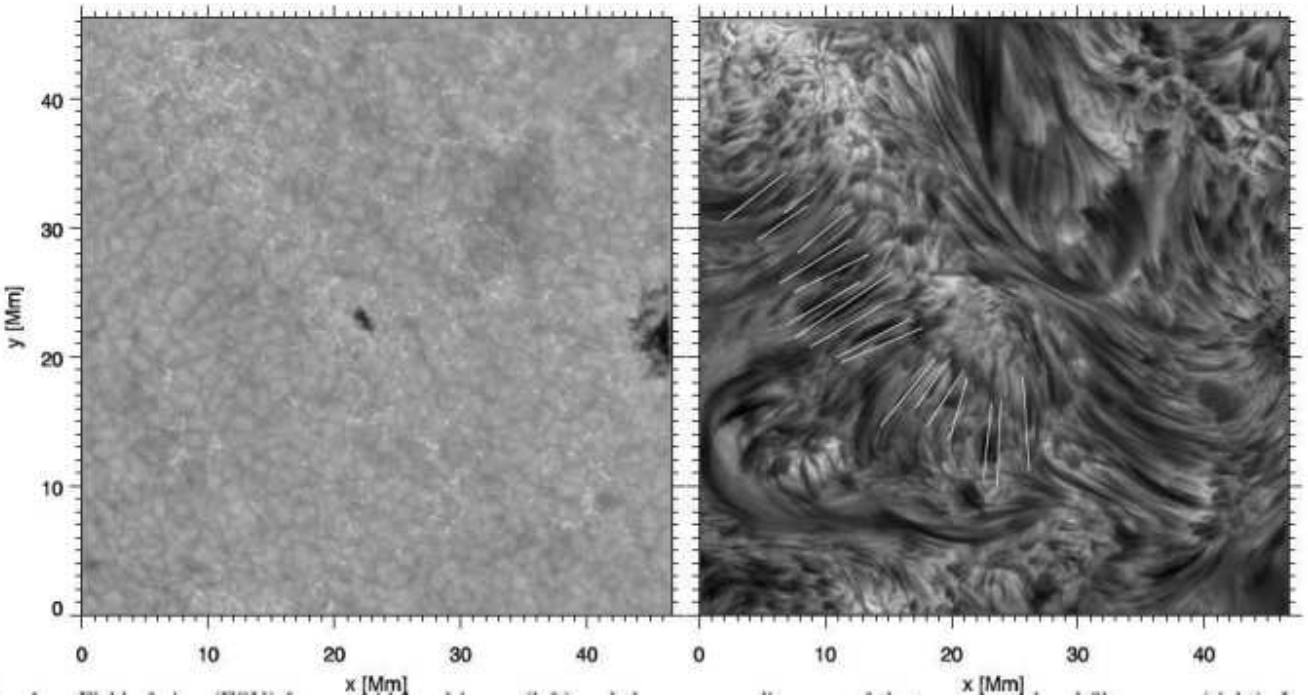


FIG. 1.— Field of view (FOV) for one wideband image (left) and the corresponding sum of the two narrow band filtergrams (right). In the narrow band image several fibrilar structures are seen, and some DF axes are marked (solid white lines) for illustrative purposes.

In this paper we add to the understanding of these jet like structures by analysis of Dopplergrams obtained in an active region close to the disk center, hence the observed jet structures are commonly known as DFs. In §2 we describe the observational program and the instrumentation. The data reduction and the calibration method is explained in §3. In §4 we present the results of our measurements. We discuss our results in §5 and finally we summarize the results in §6.

2. OBSERVING PROGRAM AND INSTRUMENTATION

The observations were obtained with the Swedish 1-m Solar Telescope (SST, Scharmer et al. 2003a) on La Palma. The degrading effects of seeing were minimized by use of the SST adaptive optics system (Scharmer et al. 2003b) and the Multi-Object Multi-Frame Blind Deconvolution (MOMFBD, van Noort et al. 2005) image restoration method. The Solar Optical Universal Polarimeter (SOUP, Title & Rosenberg 1981) provided narrow band images in the Hα line (filter FWHM 12.8 pm). The optical setup is described in detail in De Pontieu et al. (2007). Three fast Sarnoff CCD cameras, operating at a frame rate of 37 frames s^{-1}, were simultaneously exposed by means of an optical chopper. One camera was operated as SOUP camera, the other two cameras were positioned as a phase-diversity pair on a beam that was split off from the main beam before SOUP but behind the pre-filter (FWHM 0.8 nm). The latter cameras provided wide-band photospheric reference images and operated as MOMFBD anchor channel.

The target area ($65''\times\ 65''$) was centered on a small pore in NOAA AR10910, positioned at S11°, W11°(observing angle $\theta = 21°$, $\mu = \cos\theta = 0.93$) on 23-Sep-2006, see Fig.1. The time series comprises 40 minutes, starting at 10:56:57 UT. The pixel scale was $0.065''$, the SST diffraction limit (λ/D) at 656.3 nm is $0.14''$or 100 km.

A wavelength calibration was performed for SOUP to compensate for several offsets like for example solar rotation. An Hα profile scan was obtained by stepping with 5 pm steps and averaging over a relatively quiet region in the vicinity of the target area. This profile scan was used to determine the line center shift in order to provide correct positioning in the wings. The profile scan is shown in Fig 2.

SOUP was alternating between the blue and red wing at ±30 pm from the Hα line core. The total acquisition time for the two line positions was 10.6 s: 1.1 s to record 40 exposures for each line position and 8.4 s for changing line position. The line position change time of SOUP is relatively long and is the limiting factor for selecting the number of points to sample the spectral line profile. We choose two line positions which is the absolute minimum for obtaining Doppler information. Improving the spectral sampling would imply unacceptably long acquisition times for which solar evolution changes would dominate the resulting line profile. Taking half a resolution element (approximately 60 km) as a limit, we expect that motions in the image plane with velocities faster than 6 km s^{-1} cause false signals in the Dopplergrams.

3. DATA PROCESSING

3.1. *Image post-processing*

All images from each SOUP cycle were jointly processed in a single MOMFBD restoration, yielding three restored images: one wide band, one Hα red, and one Hα blue wing image. Each restoration is based on a total of 240 frames, 80 for each camera. The sequential recording of the wing images and the long line position change time imply that the seeing for the two positions is different. For the construction of a Dopplergram from unprocessed images, one would expect significant false signals due to misalignment. However, using the

wide band cameras as MOMFBD anchor channel, the restored Hα wing images are guaranteed to be precisely aligned. The resulting Dopplergram is therefore virtually free from misalignment errors. This advantageous feature of restoring multiple objects with MOMFBD is discussed in detail in van Noort et al. (2005). Note however that significant changes in the amount of blurring can result in false signals after the subtraction process. For our data, we regard this as only a minor source of error since the seeing was stable and homogeneous.

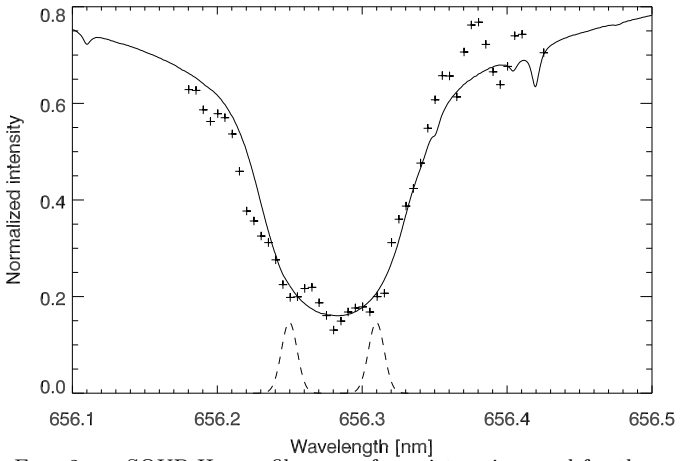


FIG. 2.— SOUP Hα profile scan of a quiet region used for the line offset calibration (crosses). A solar atlas profile is shown as reference (solid line). Furthermore, the idealized filter profiles for the red and blue wing positions are plotted on an arbitrary scale (dashed lines).

Dopplergrams D are constructed following the standard method

$$D = \frac{B - R}{B + R} \ . \tag{1}$$

with B and R being the blue and red wing images respectively. The measured pixel values in the Dopplergrams will from now on be referred to as the Doppler signal. The sum of the wing images gives an image that is reminiscent of an Hα line core image. We use these summed images as substitutes for line core images to measure the DF trajectories.

The wide band and wing images form a time sequence with a cadence of 19.1 s. The frames in each time series are aligned and de-stretched using the wide band images as reference to determine the (local) offsets which were then applied to the wing images. After alignment and de-stretching, Dopplergrams and summed images are constructed from the wing images.

3.2. *Dopplergram calibration*

The Dopplergrams were calibrated in order to interpret the signals as Doppler velocities. The main concern with such a calibration is the large variation in the shape of the Hα line profiles from different regions of the Sun.

As a first order approach we use the Hα atlas profile from the Kitt Peak solar spectral atlas (Brault & Neckel 1987). Artificial Doppler shifts are applied to the atlas profile, and the Doppler signals are measured, using the same procedures as for the observations. For low velocities, there is a linear correlation between the velocity and the Doppler signal. For velocities approaching 13.7 km s^{-1}, the velocity corresponding to a Doppler shift of 30 pm, the correlation starts to deviate from linear. Only for velocities that follow the linear correlation with the Doppler signal, a simple calibration constant can be used. We estimate that for the line positions used, $\pm$30 pm, this corresponds to a velocity of about 9 km s^{-1}, or a Doppler signal of $\pm$ 0.4.

The atlas profile is derived from averaging observations from disk center quiet Sun. The calibration constant derived from this profile might not necessarily apply to Doppler observations from other solar structures. To investigate the effect of variations in the shape of Hα line profiles on Doppler signals we analyze spectrogram timeseries of both quiet Sun and an active region.

The quiet sun spectral timeseries was obtained on the same day, 04-May-2006, as the active region time series described in paper 1. This timeseries covers about an hour of a fairly quiet internetwork region at disk center, obtained during excellent seeing conditions. As for the spectral atlas, we measure both the Doppler velocity and the Doppler signal, but now we measure this in the resolved spectra. The observed Hα line profiles are generally very wide and flat and have therefore rather low Doppler sensitivity. To cope with these problems the Doppler velocity was measured using the center–of–gravity (COG) shift of the 4% lowest intensity of the line. This method gives more weight to the Doppler velocities from the near wings, similar to the Doppler signal measurement. The resulting correlation between the Doppler signal and the Doppler shifts is shown in panel b in Fig. 3. It is clear that the result from the quiet Sun series is very similar to the relation found for shifting the atlas profile. This is because the width of the resolved line profiles in this region do not differ substantially from the atlas profile.

The active region spectral timeseries is described in detail in paper 1. This series covers a plage region containing several pores. The viewing angle ($\mu = 0.96$) is approximately the same as the angle in the Dopplergrams from the present paper, hence any systematic errors introduced by differences in the viewing angle are small. As above, both the Doppler velocity and the Doppler signal are measured in this timeseries. Significant differences compared with the spectral atlas calibration are found, see Fig.3 panels c–d. The calibration constant is in general higher in the active region, typically by a factor two. It is, however, clear from the spatially resolved calibration constants (panel c in Fig.3), that the variation is quite large. This variation is caused by the different spatial structures covered by the slit. The lower and middle part of panel c) covered pores hosting running penumbral waves, the upper part covered low lying fibrils. In these regions, smaller calibration constants are found. In the boxed areas of panel c), there is also some variation, but the lowest values are always substantially higher than for the quiet sun. These areas hosted several dynamic fibrils. Similar results were found in other time series, but with slightly lower calibration constants. We attribute this to the seeing conditions, which were less favourable.

We conclude that observed Doppler signals are very dependent on the shape of the Hα line profile. The shape of the line profile varies significantly for different solar

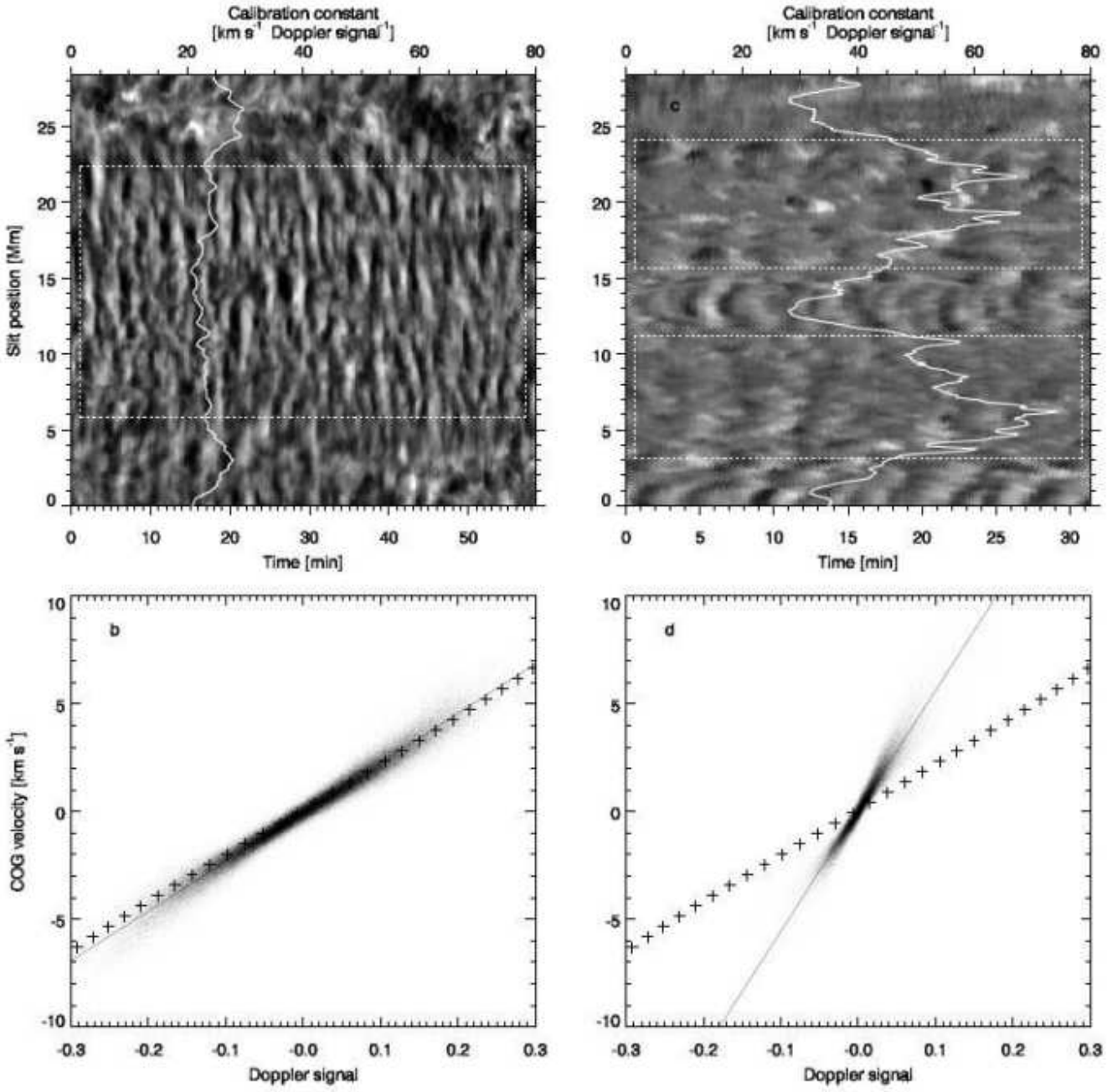


FIG. 3.— Relation between Doppler signal and velocity. The Doppler signals of a quiet Sun spectrogram time series are shown in grey scale in panel a). White corresponds to upflow and dark to downflow respectively. The white solid line shows the spatially resolved calibration constant derived from the temporal spread at that location (top axis). The boxed area in panel a) covered internetwork, the top and bottom parts mottles. The scatter plot of the Doppler signal and the COG velocity from the boxed area in panel a) are shown in panel b). The least squares linear fit (solid line) as well as the artificially shifted atlas profile (crosses) are seen. An active region timeseries is shown in panel c). The two regions known to contain DFs are indicated by the two boxes. The three excluded regions contain (lower and middle) running penumbral waves, and (upper) long fibrils. Again the calibration constant, assuming zero offset, is indicated (solid line). The scatter-plot obtained from the two boxed regions in panel c is seen in panel d). The least squares linear fit (solid line) as well as the artificially shifted atlas profile (crosses) are seen.

be done with care. The use of spatially resolved spectra is highly desirable, but even then the variations can be quite high. For the remainder of this paper we adapt a calibration constant of 55 km s^{-1} Doppler signal^{-1} , the mean value from the two boxes in panel c in Fig. 3. We argue that the calibration constant from these boxes is the optimal choice for our Dopplergrams since we are interested in DFs. Numerous DFs were found in the region of the calibration constants in these resolved spectra is 7 km s^{-1}. Note that this error should be multiplied by the Doppler signal, which gives a typical error of about 1–1.5 km s^{-1}.

3.3. *Trajectory measurement method*

For the measurement of the line of sight (LOS) Doppler

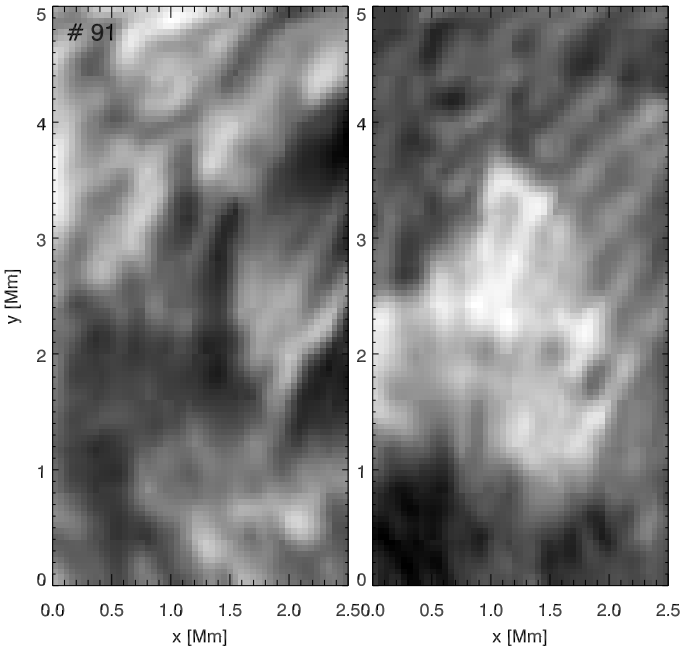


FIG. 4.— Example of an intensity image of a group of DFs (left panel), and the corresponding Doppler signal (right panel). In the Dopplergram, black and white signify upflow and downflow respectively. A movie of this DF is supplied in the electronic version of this paper.

De Pontieu et al. (2007). The DFs are identified by visual inspection of the summed intensity time series, and DF axes are manually defined. We see that individual DFs follow approximately straight trajectories. The right panel in Fig. 1 shows examples of such axes, see also Fig.4 for a more detailed view of a DF. Data along these axes is extracted from both the summed and Doppler data 'cubes' for further analysis. From the extracted data we construct x–t plots for measuring DF trajectories. Some examples of x–t plots showing both the intensity and the Doppler signal are seen in Fig.5.

The trajectory is defined by the position of the maximum change in the intensity between the top of the DF and the background, and a parabola is fitted to these data points. These parabolic fits give a good description of the temporal evolution of the length of the DFs, see Fig.6. The velocity in the image plane is given by the time derivative of the fitted parabola.

The Dopplersignal is extracted from the Dopplergrams, using the positions given by the parabolic fits obtained from the filtergrams. For a more robust measurement of the Doppler signal, we extract the Dopplersignal 5 pixels (235 km) below these points along the DF axis, for further discussion, see § 3.4. The Doppler data are fitted with a linear least square fit, which gives a good description of the time evolution of the velocity, see Fig.6. The maximum velocity and deceleration is derived from the linear fit.

3.4. *Error estimation*

In this section we summarize the different sources of error and discuss to what extent these affect our measurements of DF trajectories. The uncertainty in the line center calibration through the SOUP profile scan af-

Fig. 2). This could introduce an offset in the Doppler velocity which affects the determination of the maximum Doppler velocity. To get a reasonable estimate on the error in this calibration, we have shifted the atlas profile relative to the observational points. Visual inspection of these shifted fits gives us an estimate of the error of the order of ± 1 km s^{-1}.

The long tuning time, 8.4 s, between the two spectral positions introduces errors due to changes in the seeing and solar evolution. In § 3.1, we argue that the error from seeing is minimal due to the favorable conditions. Furthermore, the MOMFBD method guarantees precise alignment of the SOUP images. In § 2, we estimate that motions in the image plane that are faster than $\approx$6 km s^{-1} cause false signals. This is a serious concern since DFs have maximum velocities that are far greater than 6 km s^{-1}. For the summed images, this means that one would expect the top end for the DFs to be less well defined during the beginning and end of their lifetime, when the velocity is largest. However, for the measurement of the DF trajectory this is of lesser concern since most of the measured points are found during the period close to maximum height when the velocity is lowest. The deceleration and maximum velocity are determined from the parabolic fit. Also in the Dopplergrams, the changes due to solar evolution mostly effect the sharp edge of the DFs and significant false signals can be expected during the periods close to maximum velocity. This is why we choose to measure the Doppler values a few pixels lower than the top of the DF. Since the DFs have considerable linear extent that appear to be moving rather coherently, we estimate that this way we reduce the effect of solar evolution on the measured maximum Doppler velocity. Like for the summed images, the deceleration is determined from a fit where most of the fitted points are found when the velocity is lowest. In the same manner, using the linear fit reduces the impact of the increasing error for larger velocities, when the velocity approaches values corresponding to the $\pm$30 pm filter offset.

As mentioned in §3.2 the calibration constant in the region where DFs are found varies, this can probably be attributed to variations in the magnetic field topology. This introduces an error of about 1–1.5 km s^{-1}. Combining all the errors in the Doppler velocity measurements gives an error of approximately 2 km s^{-1}. The proper motion velocities has an error of about 1 km s^{-1}.

4. RESULTS

A total of 124 DFs are identified throughout the 40 minute time series. One example of a group of DFs is seen in Fig.4. These DFs are seen to move in a semi-coherent manner, as illustrated by the Dopplergram which displays downflow signal for the whole patch of DFs. Such semi-coherent behavior of groups of DFs is also described in De Pontieu et al. (2007).

TABLE 1
STATISTICAL PROPERTIES OF DFS.

Life time [s]	Proper vel. [km s^{-1}]	Proper dec. [m s^{-2}]	LOS vel. [km s^{-1}]	LOS dec. [m s^{-2}]
258 $\pm$ [56]	18.6 $\pm$ [6.6]	142 $\pm$ [64]	6.4 $\pm$ [2.1]	33.7 $\pm$ [15.6]

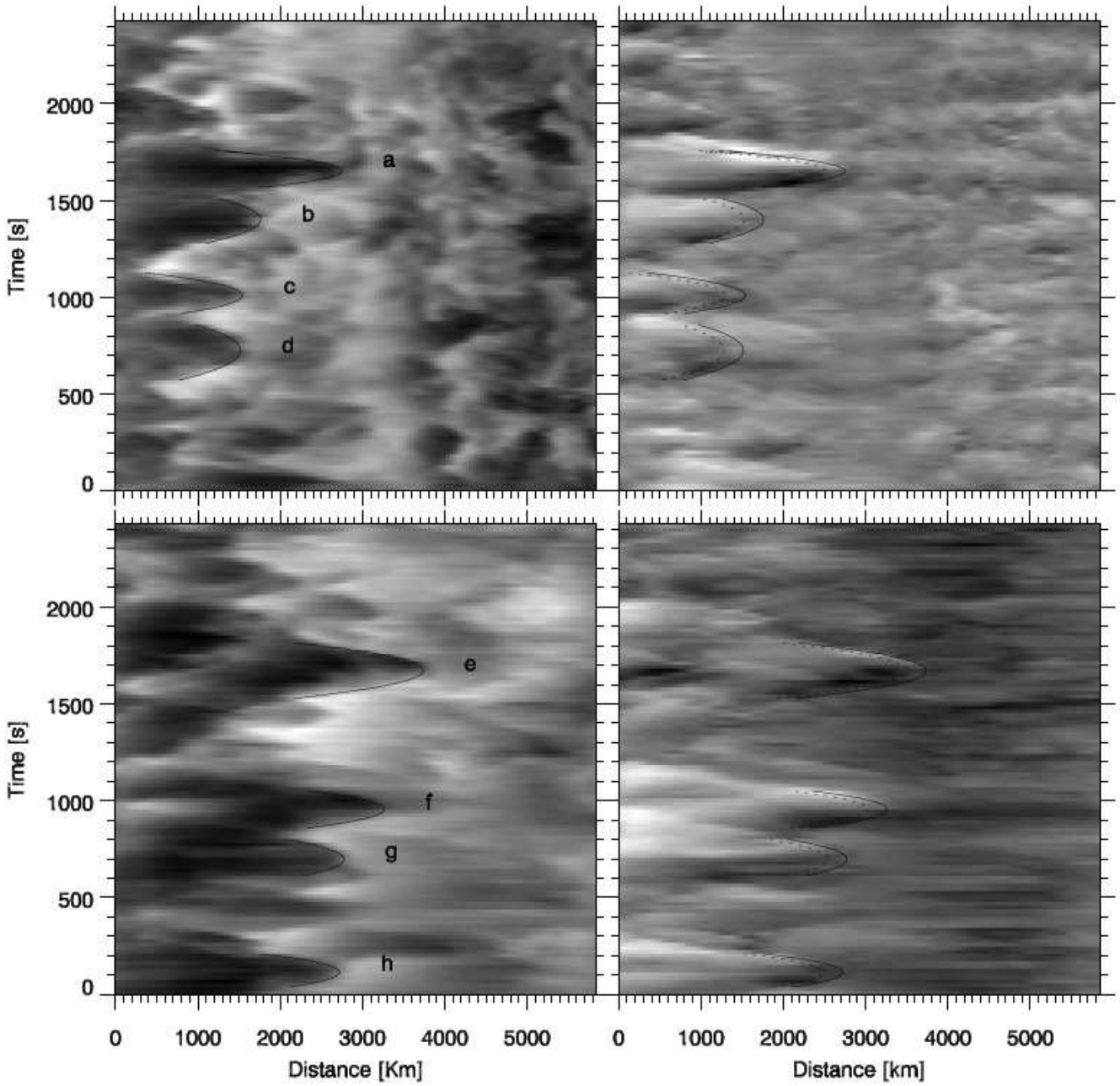


FIG. 5.— Two illustrative examples of summed x–t plots are seen in the upper and lower left panels. The corresponding Dopplergrams are seen in the two panels to the right. The parabolas fitted in the intensity image (solid) and the parabolas used in the Doppler images (dashed) are seen. Each parabola is marked with a letter which corresponds to the individual DF plots presented in Fig.6.

imum velocities, decelerations, and lifetimes of the 124 DFs, both in the image plane and along the LOS. For the Doppler measurements we include only those with an increasing velocity with time, and with a change in velocity of more than 3 $\mathrm{km\,s^{-1}}$ over the DFs lifetime. Using these criteria we remove 18 DFs, which means that more than 85% of the DFs display clear Doppler shifts together with proper motion. The statistical properties extracted for these DFs (124 based on proper motion and 106 based on Doppler motion) are presented in Table.1. The mean values are showed together with the corresponding standard deviations in brackets.

The deceleration and the maximum velocity show a strong correlation both in the image data and the

5. DISCUSSION

The correlation between the maximum velocities and decelerations found from the proper motion measurements is similar to the correlation found by Hansteen et al. (2006) and De Pontieu et al. (2007). This is illustrated in Fig. 7 by the grey-scaled cloud shown in the background. This correlation between the deceleration and the maximum velocity is known to be the signature of shock waves being the driving mechanism of DFs (Hansteen et al. 2006; De Pontieu et al. 2007; Heggland et al. 2007).

Further support for this driving mechanism comes from the fact that we find a coherent behavior between the

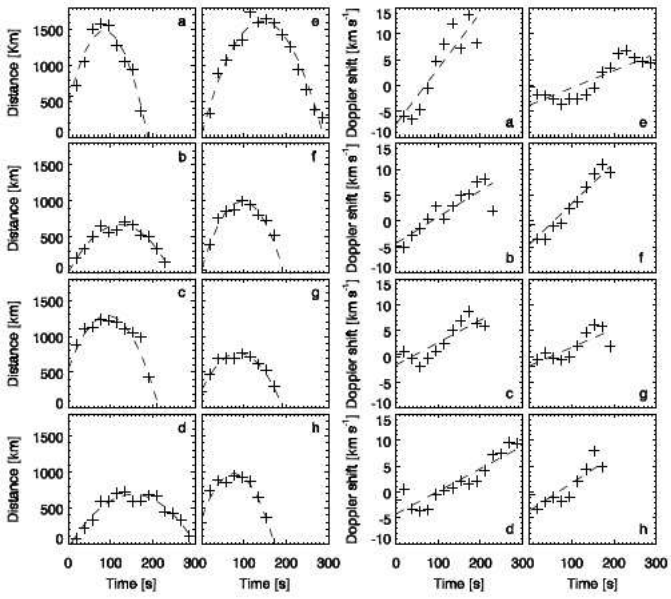


FIG. 6.— For illustration of our observations we have plotted eight examples of measured DFs. The eight panels to the left show the intensity fitted parabolas, while the eight panels to the right show the corresponding Doppler shifts. The letters in each panel makes it possible to identify the corresponding DFs seen in Fig.5.

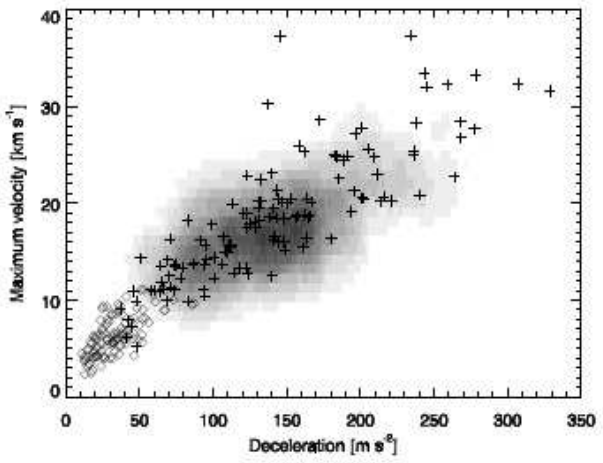


FIG. 7.— Scatter plot of the decelerations and maximum velocities. The earlier reported values Hansteen et al. (2006) is shown (scatter cloud). The image data results (crosses) and the Doppler data results(diamonds) are over plotted.

a large fraction of the DFs. This is a strong indication that there is actual plasma motion occurring during the life time of DFs. This supports the findings of paper 1, but based on a much larger sample.

The Doppler measurements show a similar correlation as for the proper motion, but with much lower absolute values for both the decelerations and maximum velocities. One possible explanation for these lower values could be high inclination angles of the DF trajectories with the LOS. One could expect to be able to derive the full trajectory vector by combining the two measured deceleration components. This naive method would give very high inclination angles, typically 75°. We know, however, that this can not be the true inclination angle. spheric velocity weighted with the response function to velocity over an extended height. In contrast, the measured proper motion is very local due to the high contrast boundary between the top of the fibril and the surroundings. Combining these two measurements leads to highly overestimated inclination angles. The difference in absolute values must be considered in the context of the results from Paper 1. The lower Doppler velocities found from the Ca II IR line was explained by a combination of lower formation height and extended formation range. This is probably also the case for the Hα line, but the formation height usually extends over a larger height range as compared to the Ca II IR line.

The lacking Doppler shifts in ∼15% of the DFs can either be caused by very high inclination angles, or their driving mechanism is fundamentally different and the evolution of these DFs is not a result of mass motion. We believe that high inclination angles combined with the uncertainties in the measurements is a more plausible explanation for the lacking Doppler signals. The identification method of DFs introduces a bias toward the more inclined DFs. There are a number of suggestive cases where DFs are visible in the Dopplergrams but no clear signature can be seen in the corresponding intensity images. We refrain from measuring these DFs since this will complicate a comparison with other data sets. Furthermore, the identification of these DFs is not objective and we expect the measurement errors to be unacceptably high since low inclination angles would lead to potentially high Doppler velocities. Due to the lacking spectral sampling this could lead to strong saturation effects in the measured Doppler velocities.

5.1. *Spicules, mottles and fibrils*

The identification of the disk counterpart of spicules was already an important question forty years ago (e.g Beckers 1968). One of the main problems was to reconcile the velocities measured in spicules with those measured in mottles. This problem was also the main concern of Grossmann-Doerth & Schmidt (1992). They conclude that since the velocities are much larger in spicules than in mottles, the two could not be the same structure seen at different viewing angles. They, however, admit that the seeing might impair their results if the structures observed were smaller than 1″. Later studies of mottles and spicule properties lead to the conclusion that spicules and mottles are in fact the same feature seen at different angles (Tsiropoula et al. 1993, 1994). Tsiropoula et al. (1994) showed, using cloud modelling, that the proper motion and the cloud velocities were consistent. In a more recent work, Christopoulou et al. (2001) use a limb darkening correction method to directly observe mottles crossing the limb. They argue that the main reason for earlier confusion is caused by the lacking spatial resolution of the observations.

In our study it is clear that the Doppler signal originates from spatially resolved structures. The excellent quality of the observations largely removes the errors due to lacking spatial resolution. Assuming reasonable inclination angles, i.e. the mean angles being not very large nor very small, we can conclude that the Doppler velocities are typically a factor of ∼ 2–3 smaller than the corresponding proper motion. A similar, but larger difference

this difference can be attributed to worse spatial resolution.

As discussed above, radiative transfer processes are the fundamental reason for the Doppler velocities being lower than the proper motion. We argue that the fundamental differences between Doppler and proper motion velocities that we find for DFs, also are valid for similar measurements on spicules and mottles. Besides the arguments of lacking spatial resolution, we believe that this difference was an important contributor to the earlier confusion about the unification of mottles and spicules. Similar work on spatially resolved limb spicules is needed to finally settle this discussion.

6. SUMMARY

With the SST we have obtained a 40 minute timeseries of an active region observed in two line positions in the Hα spectral line. For the first time, proper motion and Doppler velocity of DFs can be simultaneously measured in spatially resolved observations.

We find that most DFs, about 85% of our sample, show both co-temporal and co-spatial Doppler motion and proper motion. The coherent behavior of the two velocity components shows that the evolution of DFs involve real plasma motion.

Both the proper motion and the Doppler measurements show a strong correlation between the maximum velocity and the deceleration. This is in agreement with earlier findings and supports the theory that DFs are driven by magneto acoustic shocks.

We derive significantly lower values for the deceleration and maximum velocity from the Doppler measurements. We argue that this can be explained by the height extension of the response function. The Doppler velocity is a result of the atmospheric velocity weighted with the response function over an extended height. The proper motion velocity is derived from the large contrast between the top of the DF and the background which is a very local measure.

Using high resolution spectrograms we have demonstrated the importance of a rigid calibration method for Dopplergrams.

Mats Carlsson is thanked for improving the manuscript. The Norwegian Research Council supports Luc Rouppe van der Voort through grant 146467/420 and Yong Lin through grant FRINAT 171012. The Swedish 1-m Solar Telescope is operated on the island of La Palma by the Institute for Solar Physics of the Royal Swedish Academy of Sciences in the Spanish Observatorio del Roque de los Muchachos of the Instituto de Astrofísica de Canarias. This research has made use of NASA's Astrophysics Data System.

REFERENCES

Beckers, J. M. 1968, Sol. Phys., 3, 367
Brault, J., & Neckel, H. 1987, Hamburg Observatory anonymous ftp: `ftp.hs.uni-hamburg.de`
Carlsson, M., & Stein, R. F. 2002, ApJ, 572, 626
Christopoulou, E. B., Georgakilas, A. A., & Koutchmy, S. 2001, Sol. Phys., 199, 61
De Pontieu, B., Erdélyi, R., & James, S. P. 2004, Nature, 430, 536
De Pontieu, B., Hansteen, V. H., Rouppe van der Voort, L., van Noort, M., & Carlsson, M. 2007, ApJ, 655, 624
de Wijn, A. G., & de Pontieu, B. 2006, A&A, 460, 309
Grossmann-Doerth, U., & Schmidt, W. 1992, A&A, 264, 236
Hale, G. E. 1908, ApJ, 28, 100
Hansteen, V., De Pontieu, B., Rouppe van der Voort, L., van Noort, M., & Carlsson, M. 2006, ApJ, 647, L73
Heggland, L., De Pontieu, B., & Hansteen, V. H. 2007, ApJ, 666, 1277
Langangen, O., Carlsson, M., Rouppe van der Voort, L., Hansteen, V., & De Pontieu, B. 2007, ArXiv e-prints, 710, Submitted to ApJ
Leenaarts, J., & Wedemeyer-Böhm, S. 2006, A&A, 460, 301
Rouppe van der Voort, L., De Pontieu, B., Hansteen, V. H., Carlsson, M., & van Noort, M. 2007, ApJ, 660, L169
Scharmer, G., Bjelksjö, K., Korhonen, T., Lindberg, B., & Petterson, B. 2003a, in Proceedings of the SPIE, Volume 4853. pp. 341-350
Scharmer, G. B., Dettori, P. M., Löfdahl, M. G., & Shand, M. 2003b, in Innovative Telescopes and Instrumentation for Solar Astrophysics. Edited by Stephen L. Keil, Sergey V. Avakyan . Proceedings of the SPIE, Volume 4853, pp. 370-380
Sterling, A. C. 2000, Sol. Phys., 196, 79
Suematsu, Y., Wang, H., & Zirin, H. 1995, ApJ, 450, 411
Title, A., & Rosenberg, W. 1981, Optical Engineering, 20, 815
Tsiropoula, G., Alissandrakis, C. E., & Schmieder, B. 1993, A&A, 271, 574
—. 1994, A&A, 290, 285
van Noort, M., Rouppe van der Voort, L., & Löfdahl, M. G. 2005, Sol. Phys., 228, 191